

Vibrational ladder-descending photostabilization of a weakly bound molecule: Quantum optimal control with a genetic algorithm

Mateo Londoño*

Departamento de Física, Universidad del Valle, A.A. 25360, Cali, Colombia

Julio C. Arce†

Departamento de Química, Universidad del Valle, A.A. 25360, Cali, Colombia

(Dated: May 13, 2022)

We propose an optical control scheme for driving a polar molecule from a high-lying vibrational level to a target low-lying one, within the same electronic state. The scheme utilizes an infrared chirped laser pulse with an analytical shape, whose parameters are optimized by means of a heuristic formulation of quantum optimal control based on a genetic algorithm. We illustrate this methodology computationally for a KRb Feshbach molecule in the lowest triplet electronic state.

I. INTRODUCTION

The formation of cold ($1 \text{ mK} < T < 1 \text{ K}$) and ultracold ($T < 1 \text{ mK}$) ensembles of diatomic molecules in a controlled fashion [1, 2] is a current challenge of great interdisciplinary interest [3–6]. Proposals have been put forth for the creation of such ensembles from the binary collisions in cold or ultracold atomic gases by one-step photoassociation (PA) [7–11], two-step PA [12], a combination of one-step and two-step PA [13], magnetoassociation [14], and electroassociation [15]. One-step PA, magnetoassociation, and electroassociation involve only one Born-Oppenheimer potential-energy curve (PEC), whereas two-step PA involves several PECs.

In all these association methods the molecules are typically left in a distribution of rovibrational levels of the ground and/or an excited electronic state. Hence, to achieve cooling, control schemes must be applied for the subsequent stabilization into low-lying rovibrational levels of the ground electronic state, including the absolute ground state. For the situation where the molecules are left in high- or intermediate-lying levels of the ground electronic state, and if they are polar, controlled stabilization schemes within the same electronic state have been devised [9, 16–19]. Of particular interest for this paper are those that entail a consecutive descend across the ladder of vibrational levels, using a single chirped laser pulse. For example, Marquetand and Engel employed local control theory to achieve one-step PA together with some stabilization during H+F and H+I collisions [9], and Devolder *et al.* applied a quantum optimal control (QOC) method for the stabilization of a RbSr molecule formed previously via one-step PA [19]. However, the resulting optimal pulse has a complicated structure, making it difficult to achieve experimentally. Regardless of whether the molecules are left in the ground or an excited electronic state, it has been demonstrated that pump-dump [20, 21] and STIRAP [19, 22, 23] methodologies can

achieve stabilization. Nevertheless, the involvement of intermediate excited electronic states can introduce complications, like fast spontaneous decay, internal conversions and intersystem crossings. Moreover, in these two schemes it may happen that the initial bound level has relatively small Franck-Condon factors for the transitions to the vibrational levels of the intermediate excited electronic states [21]. Therefore, in this situation it is convenient to introduce a prior step to drive the molecules to the lower-lying levels with the highest Franck-Condon factors.

In this paper, we demonstrate that QOC based on genetic algorithms (GAs) is an attractive alternative to accomplish vibrational ladder descending (LD) into a target level of a polar molecule, employing a linear chirped pulse (LCP) with an analytical shape that can be achieved experimentally with relative ease. In Sec. II we explain our LD method in the context of the model of Ref. 21, where a weakly bound KRb Feshbach molecule in the lowest triplet electronic state is driven to a lower-lying vibrational level to optimize a subsequent pump-dump stabilization scheme. In Sec. III we briefly describe the numerical methods we utilized for solving the time-independent and time-dependent Schrödinger equations, and the QOC+GA methodology we employed for the optimization of the analytical pulse shape. In Secs. IV A and IV B we present and discuss the simulation results for one-rung-at-a-time (OLD) and multiple-rung-at-a-time (MLD) variants of LD, respectively. Finally, in Sec. V we state the conclusions of this work and suggest some perspectives for future developments.

II. THE LADDER-DESCENDING SCHEME

Arango and coworkers [21] implemented a pump-dump scheme for the vibrational stabilization into the electronic ground state, $X^1\Sigma^+$, of a model $^{39}\text{K}^{87}\text{Rb}$ Feshbach molecule formed in the lowest electronic triplet state, $a^3\Sigma^+$, using the $[b - A]$ scheme that involves the spin-orbit-coupled intermediate electronic states $b^3\Pi$ and $A^1\Sigma^+$ [23]. The pump pulse stimulates the $b^3\Pi \leftarrow a^3\Sigma^+$

* mateo.londono@correounivalle.edu.co

† julio.arce@correounivalle.edu.co

absorption and the dump pulse stimulates the $A^1\Sigma^+ \rightarrow X^1\Sigma^+$ emission. Gaussian LCPs optimized by means of a GA were employed, either without (direct mechanism) or with (assisted mechanism) explicit consideration of the dynamics of the $b^3\Pi \rightarrow A^1\Sigma^+$ spin-orbit-induced radiationless transition. The molecule was considered to be initially in high-lying vibrational levels, where it may be formed through Feshbach tuning. Unfortunately, for driving the molecule into its absolute ground state, $|X^1\Sigma^+, v=0\rangle$, using this scheme such levels are far from optimal, since their (inter-curve) dipole couplings with the vibrational levels of the intermediate state $b^3\Pi$ are weak. It turns out that the strongest inter-curve couplings occur for the $v=10$ level. Hence, it is desirable to drive the molecule down to this level before applying the pump pulse. However, a direct transition is not feasible, due to the (intra-curve) dipole coupling between well-separated levels being too weak. In this paper we illustrate our infrared LD scheme by addressing this issue. Specifically, we show that this scheme allows us to bring the molecule from the initial levels $|a^3\Sigma^+, v=20, 24\rangle$ to the optimal initial level $|a^3\Sigma^+, v=10\rangle$.

The idea behind our LD scheme can be viewed as the reverse of the ladder-climbing scheme proposed by Chelkowski *et al.* [24]: The molecule is successively driven from the initial level $v=i$ down the ladder $i-1, i-2, \dots, f$, where $v=f$ is the target level, employing a single LCP. We employ a QOC method to adjust the parameters that define the shape of this pulse so as to maximize the sequential population transfer between the ladder rungs. This is possible in heteronuclear diatomic molecules where the permanent electric dipole moment, $D(R)$, provides a significant coupling between adjacent levels. To assess such coupling, we examine the squared dipole matrix elements (SDMEs) within the $a^3\Sigma^+$ electronic state,

$$D_{v,v'} \equiv |\langle v | D | v' \rangle|^2. \quad (1)$$

Figure 1(a) displays the corresponding SDME map. It can be observed that, indeed, the coupling of the level $v=10$ with the levels $v>16$ is very weak. Moreover, it can be seen that the dipole coupling between adjacent levels is relatively strong, except that around $v=14$ there is a “hole” in the coupling map, as can be more clearly appreciated in Fig. 1(b), where such hole is zoomed in. Since this can represent a problem for an OLD scheme, we also consider a MLD scheme, where this hole is skipped.

III. METHODOLOGY

We used the KRb $a^3\Sigma^+$ PEC, $V(R)$, and $D(R)$ reported in Ref. 23. We calculated the vibrational eigenenergies and eigenfunctions of the $^{39}\text{K}^{87}\text{Rb}$ isotopologue by numerical integration of the time-independent nuclear

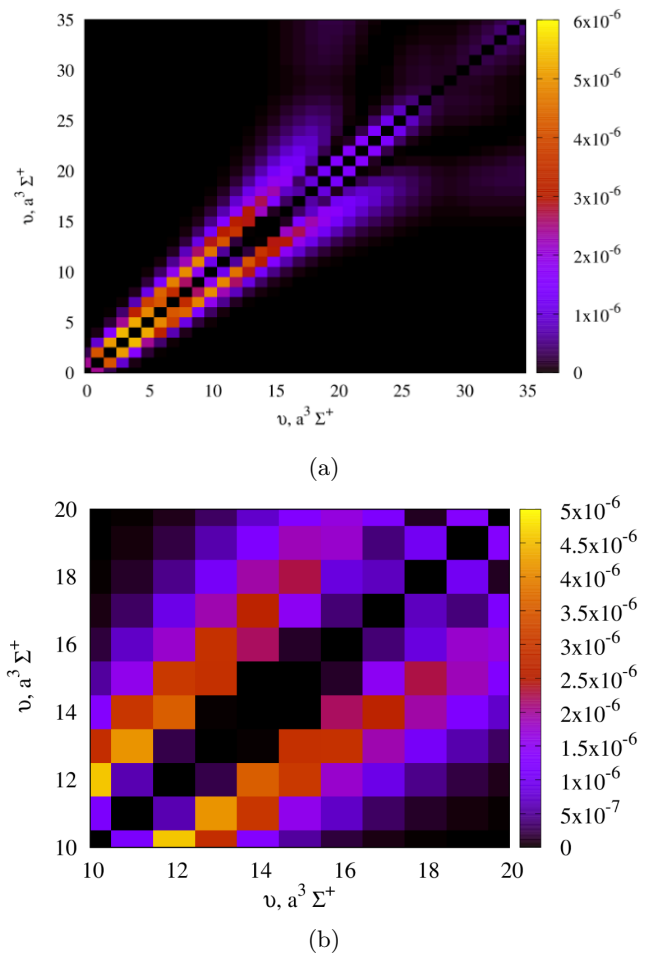


FIG. 1: (Color online) (a) Squared dipole matrix element map (in atomic units) of the $a^3\Sigma^+$ potential energy curve of KRb. (b) Zoom of the “hole” around $v=14$.

Schrödinger equation,

$$\left[-\frac{\hbar^2}{2\mu} \frac{d^2}{dR^2} + V(R) - E_v \right] \psi_v(R) = 0, \quad (2)$$

where μ is the reduced mass of the nuclei, using a Colbert-Miller discrete variable representation (DVR) [25]. Then, we evaluated the SDMEs (1) by numerical quadrature.

Within the semiclassical dipole approximation, the time-dependent nuclear Schrödinger equation takes the form

$$\left[-\frac{\hbar^2}{2\mu} \frac{d^2}{dR^2} + V(R) + \varepsilon(t)D(R) - i\hbar \frac{\partial}{\partial t} \right] \Psi(R, t) = 0. \quad (3)$$

where $\varepsilon(t)$ is the electric-field amplitude. We integrated this equation numerically, representing the wave function on a space-time grid and approximating the short-time evolution operator by means of the midpoint quadrature

and the symmetric Strang splitting,

$$\hat{U}(t_n, t_{n+1}) \approx e^{-i\hat{T}\delta t/2\hbar} e^{-iW(\bar{t}_n)\delta t/\hbar} e^{-i\hat{T}\delta t/2\hbar}, \quad (4)$$

where $\delta t \equiv t_{n+1} - t_n$ is the time step, $\bar{t}_n \equiv t_n + \delta t/2$ is the midpoint time, \hat{T} is the kinetic-energy operator, and $W(t) \equiv V(R) + \varepsilon(t)D(R)$ is the effective time-dependent potential. This approximation is accurate to $\mathcal{O}(\delta t^3)$ [26].

Since the interaction with the field can induce absorption above the dissociation threshold, besides stimulated emission, part of the wave function can escape into the continuum. When the latter reaches the end of the grid, an artificial reflection occurs that introduces a spurious back-emission into the bound levels. To avoid this effect, we added a complex absorbing potential (CAP) [27] in the asymptotic region, with the form

$$V_A(R) = -i\eta(R - R_0)^2, \quad (5)$$

where R_0 is the grid point at which this potential starts acting.

The electric field of the LCP has the Gaussian shape [26]

$$\varepsilon(t) = \varepsilon_0 \exp\left[-\frac{(t - \tau_0)^2}{2\tau^2}\right] \times \cos\left[\omega_0(t - \tau_0) + \frac{1}{2}C(t - \tau_0)^2\right], \quad (6)$$

where ε_0 and ω_0 are the central amplitude and frequency, τ_0 and τ are the time shift and width, and $C = d\omega/dt$ is the chirp parameter, with $\omega(t) = \omega_0 + C(t - \tau_0)$ being the instantaneous frequency. In this particular case, the energy difference between successive levels increases, hence $C > 0$.

To find the optimal LCP parameters, we adapted the QOC+GA methodology of Arango and coworkers [21, 26]. The i -th individual is a pulse whose chromosome consists of the 5-vector of genes $\gamma_i \equiv (\varepsilon_0, \omega_0, \tau_0, \tau, C)$. We chose an initial population of 40 individuals, according to the criteria explained below. Then, we evolved this population through the following optimization cycle: (1) Propagation of the initial wave function $\Psi(R, 0) \equiv \psi_i(R) \rightarrow \Psi(R, t_{max})$ with each one of the pulses separately, and calculation at t_{max} of their scores with the fitness function and of the cumulative fitness of the entire population. For the fitness function we chose the survival probability of the target level,

$$J = |\langle f | \Psi(t_{max}) \rangle|^2. \quad (7)$$

(2) Elimination of the individuals with fitness less than the cumulative fitness. (3) Elitist selection of the best five survivors of step (2). (4) Replacement of the eliminated individuals with the children generated by crossing over the genes of the survivors with probability Π_X , using the roulette-wheel selection method. (5) Sampling of the mutation probability of all genes of each individual of the new population, followed by mutation of those with

probabilities less than Π_M . This operation is not applied to the individuals selected in step (3). (6) Return to step (1) if the number of generations is less than 10.

To generate the initial population of LCPs, we chose the initial parameters randomly within appropriate ranges, which were determined heuristically appealing to physical considerations, as follows. The spectral bandwidth of the LCP [28]

$$\sigma = 2\sqrt{2 \ln 2} \sqrt{\frac{1}{\tau^2} + \tau^2 c^2}, \quad (8)$$

must include at least the range of frequencies required for the successive transitions, $\Delta\omega \equiv \omega_{f-1,f} - \omega_{i,i-1}$, where $\omega_{f-1,f}$ and $\omega_{i,i-1}$ are the frequencies of the last and first transitions, respectively, in the LD scheme. We set $C \approx \Delta\omega/6\tau$, hence this bandwidth takes the form

$$\sigma \approx 2\sqrt{2 \ln 2} \sqrt{\frac{1}{\tau^2} + \frac{\Delta\omega^2}{36}}. \quad (9)$$

The condition $\sigma \sim \Delta\omega$ allows us to estimate a lower bound for τ . Then, we chose τ_0 to be about three times the standard deviation of the Gaussian in Eq. (6). We made sure that the values of τ and τ_0 be much shorter than the radiative lifetime of the initial vibrational level (the lifetimes of the lower-lying levels are longer), $\tau_i = \sum_{v < i} A_{iv}^{-1}$, where $A_{iv} = 2\omega_{iv}^3 D_{iv}^2 / 3\epsilon_0 c^3 \hbar$ is an Einstein coefficient, with ω_{iv} being a transition frequency. Since $\omega(t=0) \approx \omega_{i,i-1}$, we get that $\omega_0 \approx \omega_{i,i-1} + \tau_0 \Delta\omega/6\tau$.

To determine the range of ε_0 we took into account that the Rabi period for any of the sequential transitions is $T \sim (\bar{\varepsilon} D_{v,v'})^{-1}$, where $\bar{\varepsilon}$ is the mean amplitude of the pulse during the transition, and that the range of T must be consistent with the range of τ . The resulting value of ε_0 must not be too high, to avoid ionization of the molecule.

To perform the numerical integration of Eq. (3), coupled with the QOC+GA pulse optimization, we adapted the computer code [29] employed in Ref. 21.

IV. RESULTS AND DISCUSSION

For the numerical integration of Eqs. (2) and (3), we obtained converged results employing a grid of 140 bohr and 5600 grid points, and a CAP with $R_0 = 100$ bohr and $\eta = 5 \times 10^{-6}$ hartree/bohr². We found 30 bound vibrational levels in the $a^3\Sigma^+$ electronic state. We obtained that the lifetime of the highest-lying vibrational level is $\tau_{v=30} \approx 13$ s.

After a few trials, we determined that suitable values for the GA probabilities are $\Pi_X = 0.25$ and $\Pi_M = 0.9$.

For the initial states $i = 20, 24$ we obtained the condition $\tau > 3.17 \times 10^5$ atomic units = 7.7 ps.

A. One-rung-at-a-time Ladder Descending

Table I presents the initial ranges, chosen in accordance with the criteria explained in Sec. III, and the optimal values, yielded by the GA methodology, of the LCP parameters. The optimal amplitudes turned out to be of the same order of magnitude as the ones reported in Ref. 16.

TABLE I: Ranges of the LCP parameters for the GA optimization and optimal values obtained in the OLD scheme. All quantities are given in atomic units.

| $i = 20$ | | | |
|-----------------|-----------------------|-----------------------|-------------------------|
| | min | max | optimal |
| τ | 1.0×10^6 | 1.0×10^7 | 9.798×10^6 |
| τ_0 | 3.3×10^6 | 3.5×10^7 | 4.104×10^7 |
| C | 4.0×10^{-13} | 5.0×10^{-12} | 6.259×10^{-13} |
| ω_0 | 3.1×10^{-5} | 3.6×10^{-5} | 3.531×10^{-5} |
| ε_0 | 1.0×10^{-3} | 1.0×10^{-2} | 8.011×10^{-3} |
| $i = 24$ | | | |
| | min | max | optimal |
| τ | 1.0×10^6 | 1.0×10^7 | 1.146×10^7 |
| τ_0 | 3.3×10^6 | 3.5×10^7 | 3.723×10^7 |
| C | 6.0×10^{-13} | 7.0×10^{-12} | 7.300×10^{-13} |
| ω_0 | 3.3×10^{-5} | 3.6×10^{-5} | 3.723×10^{-5} |
| ε_0 | 1.0×10^{-3} | 1.0×10^{-2} | 9.168×10^{-3} |

The optical spectrum of the LCP is given by

$$I(\omega) = \sqrt{\frac{\tau^4}{1 + c^2\tau^4}} \varepsilon_0^2 \exp \left[-\frac{(\omega - \omega_0)^2}{2\sigma^2} \right]. \quad (10)$$

Figure 2 displays the optical spectra of the LCPs for the two initial levels. It is seen that the range of excited frequencies is of the order of 10^{12} Hz, that is, in the infrared region, as expected for vibrational transitions.

Figure 3 shows the populations

$$p_v(t) = |\langle v | \Psi(t) \rangle|^2, \quad (11)$$

for the case where the initial level is $v = 20$. It is observed that, once the pulse begins to act on the system, the population is transferred down the ladder of levels in an approximately sequential manner. Naturally, the transfer between any pair of levels cannot be complete, since the pulse amplitude and chirped frequency cannot fulfill exactly the conditions required for a full population transfer in a two-level system. However, the initial level is totally emptied before the pulse is over.

At the end of the pulse, the population in the target level is $p_{v=10} = 25\%$, while a large portion of the remaining population remains in level $v = 15$. In Fig. 1 it can be appreciated that this level is at the edge of the “hole” in the SDME map, thus causing a bottleneck for the population transfer towards lower-lying levels.

The final populations in the bound levels add up to only 55%. The population loss is attributed to the afore-

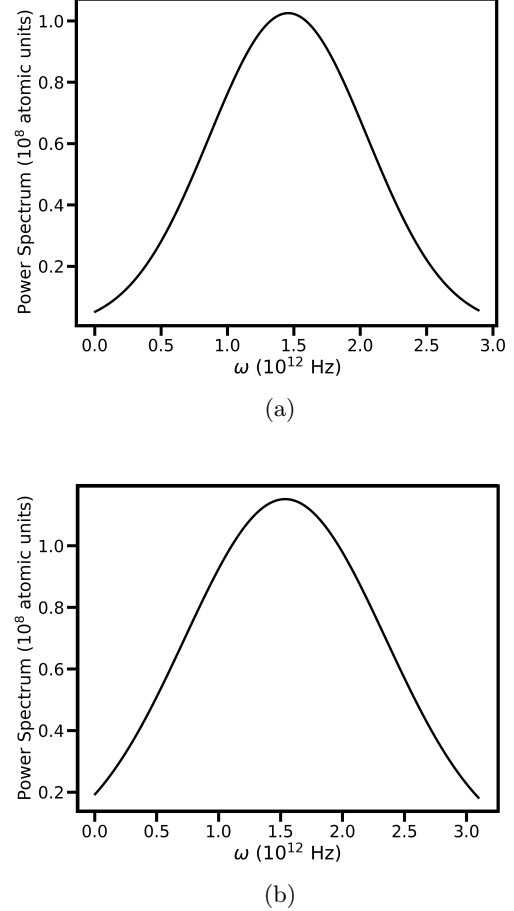


FIG. 2: Optical spectra of the optimal pulses in the OLD scheme for the two initial levels, $v = 20$ (a) and $v=24$ (b).

mentioned dissociation that results from absorption, especially at early stages of the molecule-field interaction. (We will discuss this phenomenon in more detail in Sec. IV B.)

Figure 4 displays the populations for the case where the initial level is $v = 24$. The LD mechanism is very clear until level $v = 15$ is reached, when the bottleneck is strongly manifested, causing that at the end of the pulse the population in the target state be only $p_{v=10} = 5\%$, while $p_{v=15} = 23\%$. The total population in the bound levels is 45%. The population lost to dissociation is now higher, as the initial level is closer to the dissociation threshold.

The explanation of the marked difference in the two cases is the following. When the initial level is $v = 20$, the system must climb down 10 levels to reach the target level, $v = 10$. Hence, the center of the hole, $v = 14$, is almost at the middle of the vibrational ladder, which is reached when the pulse amplitude is at its maximum, $\varepsilon(\tau_0)$. Consequently, the low coupling between adjacent states within the “hole” is compensated by the high field

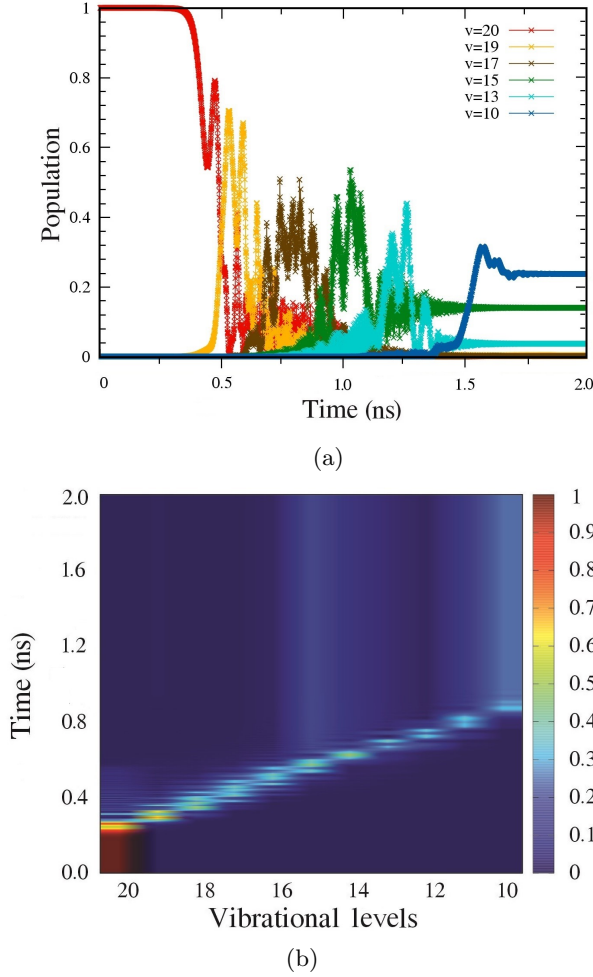


FIG. 3: (Color online) Time evolution of the populations in levels $20 \leq v \leq 10$ in the OLD scheme when the initial level is $v = 20$. (a) Selected levels. (b) All levels.

amplitude, permitting a significant population transfer before the chirp takes the field out of resonance. On the other hand, when the initial level is $v = 24$ the system must climb down 14 levels to reach the target level, and this matching cannot occur. Since in a general situation such mismatch cannot be avoided, we next explore a strategy where the system is made to “jump over the hole”.

B. Multiple-rung-at-a-time Ladder Descending

For the MLD variant we chose four (non-adjacent) levels, skipping the “hole” at $v = 14$. These must satisfy two conditions: subsequent levels exhibit a relatively strong coupling and the energy differences increase down the ladder, so that $C > 0$. (The levels could be chosen so that the energy differences decrease and $C < 0$, but this would imply that the energy difference between the first two lev-

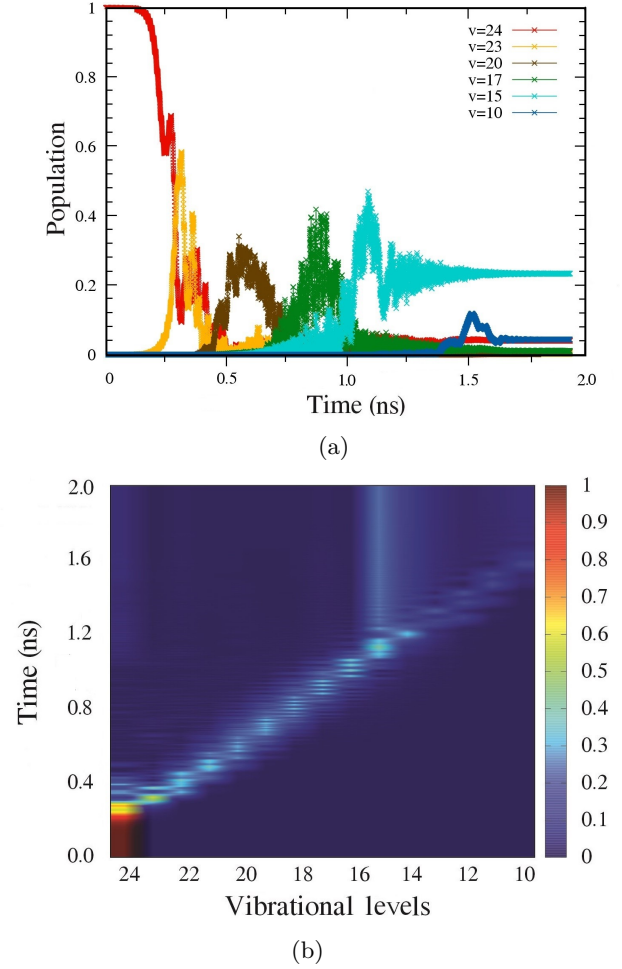


FIG. 4: (Color online) Time evolution of the populations in levels $24 \leq v \leq 10$ in the OLD scheme when the initial level is $v = 24$. (a) Selected levels. (b) All levels.

els had to be relatively large, which in turn would imply that the dipole coupling for the first transition would be relatively weak, thereby probably rendering the process to be less efficient.) The selected transitions and their energies for both initial states are shown in Table II.

TABLE II: Selected transitions in the MLD scheme for the two initial states. Energy differences are given in atomic units.

| $v_0 = 20$ | | $v_0 = 24$ | |
|---------------------|------------------------|---------------------|------------------------|
| $v \rightarrow v'$ | ΔE | $v \rightarrow v'$ | ΔE |
| $20 \rightarrow 16$ | 1.068×10^{-4} | $24 \rightarrow 17$ | 1.372×10^{-4} |
| $16 \rightarrow 13$ | 1.110×10^{-4} | $17 \rightarrow 13$ | 1.423×10^{-4} |
| $13 \rightarrow 10$ | 1.378×10^{-4} | $13 \rightarrow 10$ | 1.430×10^{-4} |

Table III displays the initial ranges and the optimal values of the LCP parameters. The optimal amplitudes

turned out to be somewhat lower than the ones of the OLD variant. Since ω_0 for the MLD scheme is an order of magnitude larger than the one for the OLD scheme, the time scale of the MLD process is one order of magnitude shorter than the one for the OLD process, as revealed by the values of τ , τ_0 , and C .

TABLE III: Ranges of the LCP parameters for the GA optimization and optimal values obtained in the MLD scheme. All quantities are given in atomic units.

| $i = 20$ | | | |
|-----------------|-----------------------|-----------------------|-------------------------|
| | min | max | optimal |
| τ | 3.2×10^5 | 3.2×10^6 | 1.489×10^6 |
| τ_0 | 1.0×10^6 | 1.0×10^7 | 4.900×10^6 |
| C | 1.8×10^{-12} | 1.6×10^{-11} | 8.254×10^{-12} |
| ω_0 | 1.0×10^{-4} | 1.8×10^{-4} | 1.211×10^{-4} |
| ε_0 | 1.0×10^{-3} | 1.0×10^{-2} | 5.154×10^{-3} |
| $i = 24$ | | | |
| | min | max | optimal |
| τ | 1.0×10^6 | 1.0×10^7 | 1.003×10^6 |
| τ_0 | 3.3×10^6 | 3.5×10^7 | 4.835×10^6 |
| C | 1.0×10^{-13} | 1.0×10^{-12} | 5.832×10^{-12} |
| ω_0 | 1.3×10^{-4} | 1.6×10^{-4} | 1.378×10^{-4} |
| ε_0 | 1.0×10^{-3} | 1.0×10^{-2} | 5.720×10^{-3} |

Figure 5 shows the optical spectra of the LCPs for the two initial levels. It can be appreciated that the range of excited frequencies is shifted towards higher values in comparison with the ones of the OLD scheme, but still is within the infrared region.

Figure 6 displays the population dynamics for the case where the initial level is $v = 24$. The LD nature of the process is evident. The final population in the target level is $p_{v=10} = 48\%$, which amounts to an increase of 43% with respect to the OLD scheme. At no time during the process is population transferred to bound levels not explicitly included in the scheme. The process takes about 0.175 ns, versus about 1.6 ns in the OLD scheme, an order of magnitude shorter, as pointed out above. The high-frequency oscillations have practically disappeared, which is a signature of the decrease in the antiresonant contributions caused by the increase of ω_0 and decrease of ε_0 , as can be inferred, for example, from the familiar expression provided by time-dependent perturbation theory for the transition amplitude, which contains the denominators $\omega_0 + \omega_{v,v'}$.

The final populations in the bound levels add up to 52%, which means that almost all the bound population was transferred to the target. Figure 7 shows the time-dependent field amplitude, total probability ($\langle \Psi(t) | \Psi(t) \rangle^2$), and dissociation probability ($1 - \langle \Psi(t) | \Psi(t) \rangle^2$). It is observed that at about 0.1 ns the total probability begins to decrease, as the CAP begins damping the continuum part of the wave function. The delay of ~ 0.05 ns with respect to the beginning of the pulse is about the time taken by such part of the wave

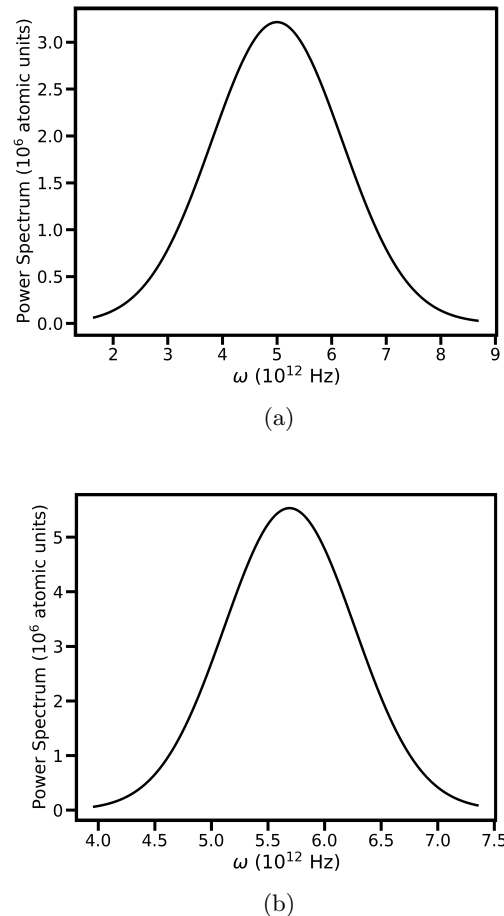


FIG. 5: Optical spectra of the optimal pulses in the MLD scheme for the two initial levels, $v = 20$ (a) and $v=24$ (b).

function to propagate to the CAP region. At ~ 0.15 ns all the continuum part of the wave function has been absorbed, and the remaining probability lies in the bound levels. Naturally, the dissociation probability mirrors the total probability.

Figure 8 shows the population dynamics for the case where the initial level is $v = 20$. Now, there appear notorious Rabi-like oscillations in the $v = 16$ and $v = 13$ populations, lasting for about 0.075 ns, although the LD nature of the process can still be appreciated. Such oscillations are complementary, indicating that the dynamics gets transiently stuck in this two-level system. The middle time of these transient oscillations is about 0.12 ns $\approx \tau_0$, which is the time when the field amplitude is at its maximum. As this two-level system decays, the population of the target level rises to a final value of $p_{v=10} = 30\%$, which amounts to an increase of only 5% with respect to the OLD scheme. This happens because by the time the target level is reached, the field amplitude is already too low. The total population in the bound levels is 40%. This case illustrates that the selection of the

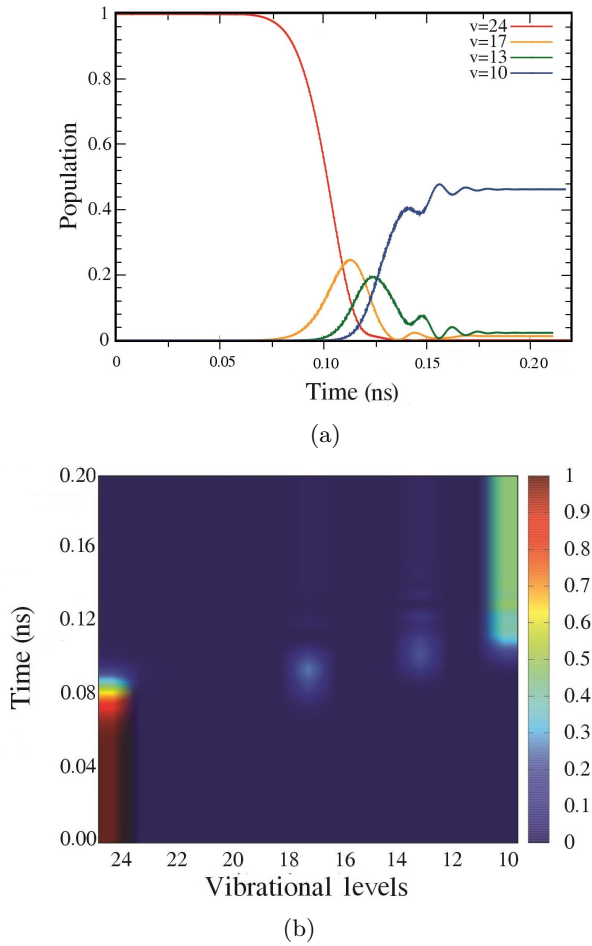


FIG. 6: (Color online) Time evolution of the level populations in the MLD scheme when the initial level is $v = 24$. (a) Chosen levels. (b) All levels.

levels constituting the ladder is crucial for the efficiency of the MLD scheme.

V. CONCLUSIONS AND OUTLOOK

We have implemented computationally an infrared ladder-descending scheme for the stabilization of a highly excited polar diatomic molecule into a given target vibrational level. The scheme employs a single linear chirped laser pulse with an analytical shape that is optimized by means of a quantum optimal control method based on a genetic algorithm. As a prototype, we considered a model KRb molecule formed by magnetoassociation in its lowest-lying triplet electronic state, $a^3\Sigma^+$ [21].

Such implementation requires some heuristics based on the dipole coupling map and the vibrational level structure of the molecule. Specifically, our prototype molecule exhibits a “hole” in the dipole coupling map that can generate a bottleneck for a one-rung-at-a-time descent down the vibrational ladder for some initial levels. We demon-

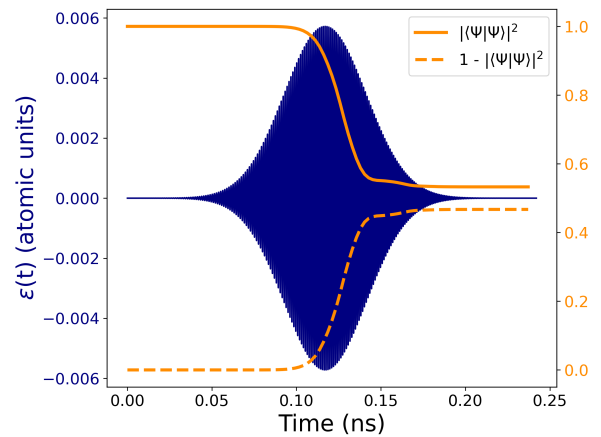


FIG. 7: (Color online) Time evolution of the optimal field amplitude and of the total bound and continuum populations in the MLD scheme when the initial level is $v = 24$.

strated that such bottleneck can be sidestepped by means of a multiple-rung-at-a-time variant of the scheme, taking advantage of the relatively strong overtones present.

Our scheme has the advantage of employing a Gaussian shape for the laser pulse, which is relatively easy to achieve experimentally. Our implementation can be improved by employing a more flexible shape, but at the obvious expense of increasing the optimization cost and the experimental difficulty. For the genetic crossing operation, we used the roulette wheel selection method. It would be worthwhile to try other selection methods that might improve the efficiency of the optimization.

Arango and coworkers have implemented a pump-dump scheme for the stabilization into the electronic ground state of this model KRb molecule, beginning from highly-excited levels of the $a^3\Sigma^+$ state, employing the same quantum optimal control methodology [21]. It turns out that beginning from certain lower-lying levels makes such process much more efficient. Hence, our vibrational stabilization scheme can be used as a “pre-pulse” for further optimization of such scheme.

The model employed does not take into account the rotational structure of the diatomic molecule. However, our previous study of the one-step photoassociation dynamics, that took into account the full rovibrational structure, revealed that for each vibrational level the rotational population distribution can become considerably wide [11]. We expect that our multiple-rung-at-a-time scheme can achieve simultaneous one-step photoassociation and cooling in this more realistic model, by hand-picking rovibrational levels in such a way that the rung separations increase (or decrease), so that a positive (or negative) frequency chirp can be employed. Work in these directions is currently underway in our laboratory.

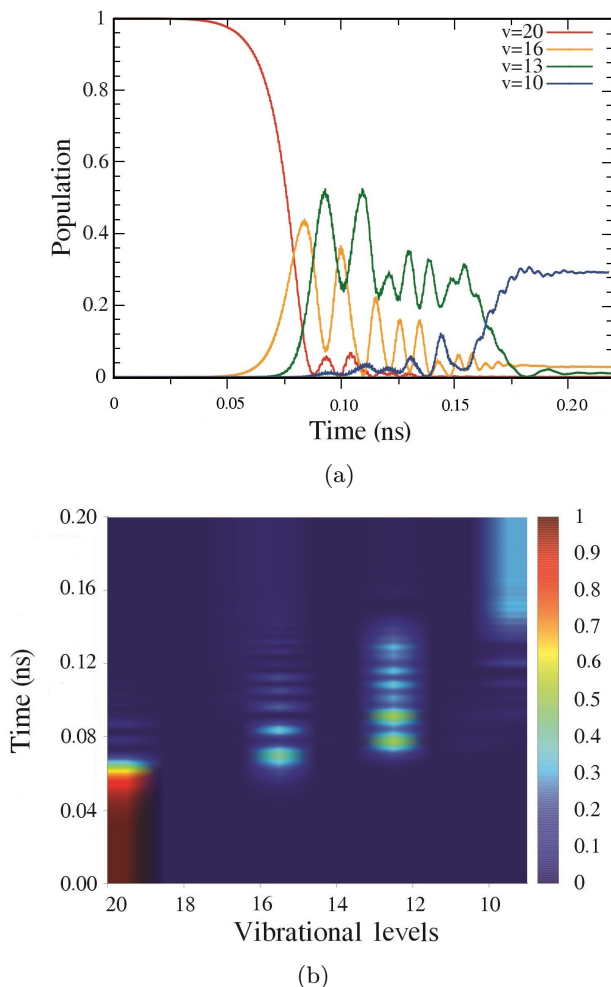


FIG. 8: (Color online) Time evolution of the level populations in the MLD scheme when the initial level is $v = 20$. (a) Chosen levels. (b) All levels.

ACKNOWLEDGMENTS

We are grateful to Diego F. Uribe and Javier Madroñero for useful discussions. M. L. is grateful to the Solid State Theory Group of Universidad del Valle for kindly providing time on their computing facilities. This work was supported in part by Colciencias through Project No. 1106-658-42793.

-
- [1] G. Quémener and P. S. Julienne, *Chem. Rev.* **112**, 4949 (2012).
 - [2] C. P. Koch, “Coherent control of cold collisions,” in *Cold Chemistry. Molecular Scattering and Reactivity Near Absolute Zero*, edited by O. Dulieu and A. Osterwalder (The Royal Society of Chemistry, Croydon, UK, 2018) pp. 633–662.
 - [3] L. D. Carr, D. DeMille, R. V. Krems, and J. Ye, *New J. Phys.* **11**, 055049 (2009).
 - [4] C. Chin, V. V. Flambaum, and M. G. Kozlov, *New J. Phys.* **11**, 055048 (2009).
 - [5] R. Côté, *Adv. Chem. Phys.* **154**, 403 (2014).
 - [6] J. Pérez-Ríos, *An Introduction to Cold and Ultra-cold Chemistry. Atoms, Molecules, Ions and Rydbergs* (Springer, Cham, Switzerland, 2020).
 - [7] E. Juarros, P. Pellegrini, K. Kirby, and R. Côté, *Phys. Rev. A* **73**, 041403(R) (2006).
 - [8] S. Kotochigova, *Phys. Rev. Lett.* **99**, 073003 (2007).
 - [9] P. Marquetand and V. Engel, *J. Chem. Phys.* **127**, 084115 (2007).
 - [10] S. Kallush and R. Kosloff, *Phys. Rev. A* **77**, 023421 (2008).
 - [11] J. S. Molano, K. D. Pérez, J. C. Arce, J. G. López, and M. L. Zambrano, *Phys. Rev. A* **100**, 063407 (2019).
 - [12] J. Ulmanis, J. Deiglmayr, M. Repp, R. Wester, and M. Weidemüller, *Chem. Rev.* **112**, 4890 (2012).
 - [13] E. F. de Lima, *Phys. Rev. A* **95**, 013411 (2017).
 - [14] T. Köhler, K. Góral, and P. S. Julienne, *Rev. Mod. Phys.* **78**, 1311 (2006).
 - [15] J. Castaño-Puerta and J. Mahecha-Gómez, *Chem. Phys.* **531**, 110651 (2020).
 - [16] M. Ndong and C. P. Koch, *Phys. Rev. A* **82**, 043437 (2010).
 - [17] E. F. de Lima, *J. Low Temp. Phys.* **180**, 161 (2015).
 - [18] Y. Niu and R. Wang, *Chin. Opt. Lett.* **16**, 060201 (2018).
 - [19] A. Devolder, M. Desouter-Lecomte, O. Atabek, E. Luc-Koenig, and O. Dulieu, *Phys. Rev. A* **103**, 033301 (2021).
 - [20] J. M. Sage, S. Sainis, T. Bergeman, and D. DeMille, *Phys. Rev. Lett.* **94**, 203001 (2005).

- [21] R. Guerrero, M. Castellanos, and C. Arango, J. Chem. Phys. **149**, 244110 (2018).
- [22] K. Aikawa, D. Akamatsu, M. Hayashi, K. Oasa, J. Kobayashi, P. Naidon, T. Kishimoto, M. Ueda, and S. Inouye, Phys. Rev. Lett. **105**, 203001 (2010).
- [23] D. Borsalino, B. Londoño Floréz, R. Vexiau, O. Dulieu, N. Bouloufa-Maafa, and E. Luc-Koenig, Phys. Rev. A **90**, 033413 (2014).
- [24] S. Chelkowski, A. D. Bandrauk, and P. B. Corkum, Phys. Rev. Lett. **65**, 2355 (1990).
- [25] D. Colbert and W. H. Miller, J. Chem. Phys. **96**, 1982 (1992).
- [26] R. Guerrero, C. Arango, and A. Reyes, J. Chem. Phys. **143**, 124108 (2015).
- [27] U. V. Riss and H. D. Meyer, J. Phys. B: At. Mol. Opt. Phys. **28**, 1475 (1995).
- [28] Y. Huang, W. Zhang, G.-R. Wang, T. Xie, and S.-L. Cong, Phys. Rev. A **86**, 43420 (2012).
- [29] “Univalle-ICESI Collaboration Code,” Original version written by R. Guerrero, 2018.